UDC 550.3:624.191.22

V. V. NABATOV[1], *Associate Professor, Candidate of Engineering Sciences, nv4@mail.ru*
A. S. VOZNESENSKII[1], *Professor, Doctor of Engineering Sciences*

[1] *National University of Science and Technology—NUST MISIS, Moscow, Russia*

INFLUENCE OF SOIL–TUNNEL LINING INTERFACE ON ITS CONTROL BY ACOUSTIC RESPONSE TO IMPULSE IMPACT

The purpose of this study is to confirm the assumption that the stress–strain behavior of soil body at the interface with lining can be the cause of the cavity formation behind the lining space. The plastic deformation zones in soil from the computer modelling geometrically agree with the locations of cavities detected by the in-situ geophysical measurements using the method of impact response. This suggests that the stress–strain behavior and transition of soil body into a plastic strain state can cause cavity formation. The cavity formation alters acoustic response of the lining to impact, which is used to detect cavities.

Keywords: *Tunnel, void, lining, NDT, FEM, plastic deformation*
DOI: *10.17580/em.2022.01.02*

Introduction

Cavity detection in the space behind the lining is very important in the construction and operation of subway tunnels. Such cavities can cause a complex stress–strain field in soil near the tunnel and in the lining itself [1], lining deformation and cracking [2, 3], rail track deformation and ground surface subsidence [4, 5]. Cavities can have a negative impact on the surrounding buildings [6].

The main technological solution to this challenge is to detect a cavity behind the lining and then provide its grouting. Since access to the space behind the lining is complicated by the lining itself (it is extremely undesirable to open it in the conditions of the operating tunnels), the cavities can be detected using geophysical methods. We can distinguish two of the most used approaches as the acoustic methods and ground penetrating radar (GPR).

GPR involves the use of electromagnetic pulses that propagate in the object, and experience reflections from heterogeneities, and change their wave shape and spectrum. GPR allows control to be implemented during repair operations [7], allows for the assessment of the thickness of the grouting layer [8], and can be used to search for cavities in the space behind the lining [9, 10] and evaluate reinforcement parameters [11, 12]. The disadvantage of GPR is the data interpretation complexity [13]. This leads to the complexity of surveying long sections of tunnels. A promising solution to this issue is to use the attribute analysis [14–19]. This is an actively evolving trend, but so far it has been poorly developed concerning the tasks described herein.

These issues are much less pronounced when using the acoustic methods. The common acoustic methods are the ultrasonic surface wave (USW), impact-echo (IE), and impulse response (IR) methods [20–23]. The USW method implies the measurement of wave velocities in the ultrasonic frequency range. This method is often used to assess the internal lining structure but is rarely applied to working with the space behind the lining [20]. In contrast, IE and IR methods are actively employed in searching cavities behind the lining.

IE relies on the detection of standing waves. The cavity, in this case, is detected by changing reflection coefficients at the lining–soil interface, which affects the standing wave generation. IR is reduced to an impact action of the lining with response detection. If the lining is not pressed by the soil, it makes more free vibrations, which increase the amplitude and decrease the detected signal fading. The attribute analysis is also being actively developed among these methods [24, 25].

Regarding the causes and consequences of cavity formation, many studies have discussed the impact of cavities on building structures, often using computer modeling. Researchers have studied strain distribution in the lining and its deformation [26–28], the effect of leaks in tunnels on deformation of the tunnels and adjacent soil [29], the long-term impact of construction technology on adjacent soil and the causes of this impact [30], and the seismic stability of the tunnel in the case of cavities behind the lining [31].

Only a relatively small number of publications concerning the causes of cavities have been published, including the studies using numerical modeling methods. The causes are often only listed in the introductions of publications. These causes are the impact of construction work, karst process development [26, 32], leaks of water into tunnels with soil washout (Leung and Meguid, 2011; Wu et al., 2020), improper grouting [2, 29] and the vibrational impact of trains and tunnel boring machines [33, 34]. From these causes, only vibrational impact and leaks are being actively studied. In the latter case, leak causes are also described, with long-term deformations of tunnel structures and poor lining quality, including violations arising during transportation and installation [29].

In such situation, it is noteworthy that the list of causes may be incomplete, while understanding the full set of causes can be important in terms of predicting the state of both a tunnel and the surrounding soil. The purpose of this study is to investigate the possibility of influencing cavity formation based on other important aspects, such as the stress–strain behavior of the soil mass near the lining and its destruction.

Methods

Our study involved both an in-field survey and numerical modeling. The date of both were jointly interpreted, which ensured validation of the modeling data and feasibility of deeper interpretation.

1. Field survey. The geophysical field survey was carried out in the tunnels of the Moscow Metro using the IR method.

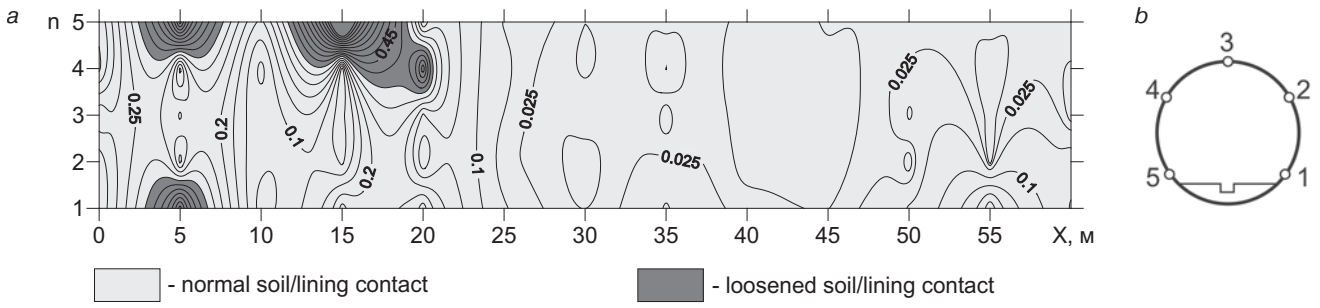

Fig. 1. Example IR survey results:
a—contact quality map; *b*—control point locations in the tunnel section (light—normal soil/lining contact; dark—loosened soil/lining contact)

The survey included points marked on the tunnel lining surface. The measurement design was five points per cross-sections spaced at 5 m. At each test point, a hit is made and a number of parameters are calculated based on the vibration response signal. Based on their analysis, a decision is made either on the presence or the absence of the cavity behind the lining. The impact point and the sensor was spaced at 30 cm. The collected data of 5 impact implementations were averaged. The parameter values at the points are plotted on the contact quality map and the values between the points are interpolated. A more detailed survey method description is given in [35, 36].

Figure 1*a* shows an example of the contact quality map at the soil–reinforced concrete tunnel lining interface. The location of measurement points is shown in **Fig. 1*b***. The numbers of these points on the *y* axis are indicated as *n*. The vertical axis of the map is plotted using the point numbers. The lower tunnel point is not usually available for survey using the IR method because the tunnel structure in this part is multi-layered due to the railway track and has a large total thickness. As a result, it is difficult to excite the bending vibrations in it.

The visualized parameter on this contact quality map is the energy parameter *E*:

$$E = \sum_{i=0}^{n_{max}} A_i^2 \Delta t,$$

where n_{max} is the final number of the signal sample, A_i is the amplitude value of an *i*-th signal sample and Δt is the time sampling interval.

When exceeding the threshold, a decision is made on the presence of loosened soil/lining contact. The thresholds themselves were obtained by IR methods on the physical lining model, which allowed for the creation of places of normal contact with the soil and cavities behind the lining.

2. Computer modeling. Computer-aided stress–strain analysis used the finite element method (FEM) in the COMSOL Multiphysics simulation environment. The model ("Stresses in soil surrounding traffic tunnel," n.d.) was used as the basis. The main goal of the modelling was to analyze the stress–strain behaviour of soil around the tunnel. The size and location of plastic deformation zones in the soil body were of particular interest.

Since the modeled object has a shape non-changing in one direction (a tunnel in soil body), a two-dimensional model was selected for the analysis. The model is based on the Drucker–Prager yield criterion. The yield surface *F* in this case is given by:

$$F = 3\alpha\bar{\sigma} + \sigma_e - K,$$

where $\bar{\sigma}$ is the hydrostatic or mean stress, σ_e is the equivalent deviatoric stress and α and *K* are the material parameters described as follows:

$$\alpha = \frac{2\sin\varphi}{\sqrt{3}(3-\sin\varphi)}; K = \frac{6c\cos\varphi}{\sqrt{3}(3-\sin\varphi)},$$

where φ is the angle of internal friction and *c* is the cohesion coefficient.

If the two-dimensional structure of the model prevails (i.e. the three-dimensional structure can be easily reduced to the two-dimensional structure), the Drucker–Prager criterion becomes identical to the Mohr–Coulomb criterion, provided that the material parameters are calculated as follows:

$$\alpha = \frac{\tan\varphi}{\sqrt{9+12\tan^2\varphi}}; K = \frac{3c}{\sqrt{9+12\tan^2\varphi}}.$$

Simultaneously, the mean stress $\bar{\sigma}$ is determined in terms of the normal stress components σ_1, σ_2 and σ_3:

$$\bar{\sigma} = \frac{\sigma_1+\sigma_2+\sigma_3}{3}.$$

The equivalent deviatoric stress σ_e is given by:

$$\sigma_e = \sqrt{\frac{1}{2}(s_x^2+s_y^2+s_z^2)+s_{xy}^2+s_{yz}^2+s_{zx}^2},$$

where s_{ij} are the components of the deviatoric stress: $s_x = \sigma_x - \bar{\sigma}$; $s_y = \sigma_y - \bar{\sigma}$; $s_z = \sigma_z - \bar{\sigma}$; $s_{xy} = \tau_{xy}$; $s_{yz} = \tau_{yz}$; $s_{zx} = \tau_{zx}$.

The soil was modeled as a homogeneous layer with a thickness of 65 m. The soil model size was 180 m wide. The tunnel was modeled as a 5.6 m diameter lining ring with a thickness of 0.3 m. The tectonic stresses, if present, can greatly change the stress distribution in soil around the tunnel and at the sollining interface [38]. We only model if gravitational stress and neglect the tectonic stress. The soil body is simulated by a uniform, isotropic and linearly deformable medium inside an elastic half-space. **Figure 2** depicts the model and describes the boundary conditions at the lateral earth pressure coefficient q = ν/(1 – ν), where ν is Poisson's ratio.

Properties of model elements. The physical properties of soil were determined from geotechnical surveys, which included a laboratory study of the soil samples. The values used are compiled in **Table**.

The modeling included additional research varying the values of the model physical parameters to determine how and to what extent they can affect the results. The work was mostly based on the method of a single-factor experiment, when one factor is varied. All the other factors were kept constant. These

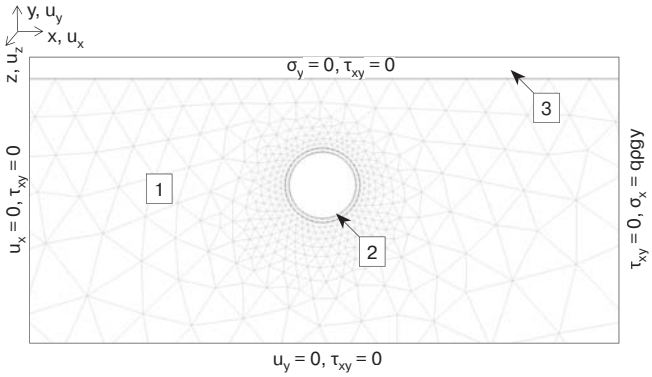

Fig. 2. Model view and mesh (688 mesh points and 1265 elements):
1—soil; 2—tunnel lining; 3—free space

Physical properties of model

	φ, deg	*C*, Pa	γ, N/m³	*E*, Pa	ν
Soil mass	36	50000	22000	$50 \cdot 10^6$	0.3
Lining	–	–	25000	$20 \cdot 10^9$	0.2

studies have shown that the modeling results are reasonably stable and only weakly dependent on the physical parameters.

Boundary conditions. "Roller"-type properties were assigned to the soil model boundaries (displacements along the boundary are allowed and displacements normal to the boundary are prohibited), excluding the boundary of ground surface with the "Free"-type property assigned (all displacements are allowed). The same type of properties was chosen for the soil–lining and lining–inner tunnel space interfaces.

The model was solved using the solver *Damped Newton*. The model calculation involved a specific approach where the values of the model parameters (Young's modulus *E* and specific weight γ) gradually increased in proportion to the **para** parameter value. The model calculation stopped if **para** reached the threshold level, while *E* and γ reached the required values. This calculation algorithm is implemented to ensure convergence of the model.

If the calculations failed to meet the convergence condition before the target levels of *E* and γ were achieved, the model was considered nonconvergent. Similar situations arose at some values of soil parameters. These cases were discarded from the further analysis.

The modeling results were visualized as maps of σ_e (equivalent deviatoric stress contour lines) and ε_{pl} (effective plastic strains visualized by a colour scale) parameters. In most cases, a binary scale was used for ε_{pl}, implying the use of two colours: $\varepsilon_{pl} > 0$ (the presence of strains) and ε_{pl} 0 (no strains). Thus, the colour map showed areas where plastic deformations and soil loosening were observed. An illustration of the results can be seen in **Fig. 3** for both the binary scale (a) and grayscale (b).

Results

Figure 3 shows the modeling results for the case of one tunnel in a single-layer soil. **Figure 3*a*** shows the threshold coding of ε_{pl} (digit 1 denotes the plastic deformation zones). In **Fig. 3*b*,** ε_{pl} is denoted using a typical gradient scale, which allows observing the point where ε_{pl} is highest (digit 2).

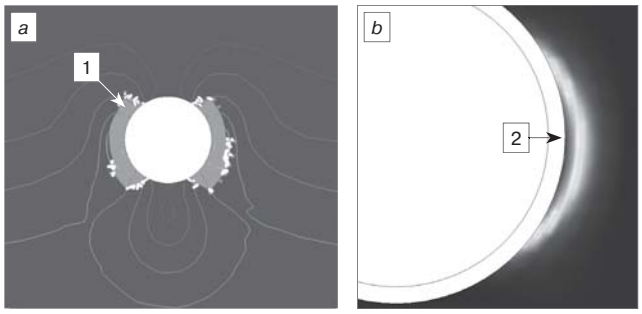

Fig. 3. Distribution of plastic deformation zones in soil near tunnel according to model calculation with original parameters:
a—results in the form of a binary scale; *b*—the same results in the form of a gradient scale; 1—plastic deformation zones, 2—maximum ε_{pl} point

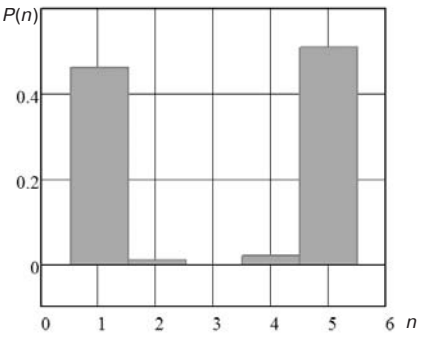

Fig. 4. Histogram of probability of cavity observation at certain tunnel points

By analyzing the resultant situation, it can be noted that plastic deformation zones occur on the left and right sides of tunnel and are almost absent at the top and bottom. This situation proved to be very stable and almost all the tried and tested model versions showed a similar pattern. Plastic deformation zones can be slightly stretched up or down, but with no fundamental changes.

Returning to the field geophysical survey in the tunnels, we can say that the analysis of a large number of contact quality maps shows that cavities occur most often at the lower points, *n* = 1 and 5. Significantly less cavities were observed at the points *n* = 2 and 4, and almost no cavities were observed at the top of the tunnel, *n* = 5. **Figure 4** shows a histogram that can be used to estimate the probability of cavity observation at certain tunnel points. The sampling included 102 values and the data were collected from six surveys on the sites corresponding to the model (tunnel diameter and shape).

Discussion

From the modeling analysis, we can deduce the following. No plastic soil deformation zones appear above the tunnel (*n* = 3). This corresponds to the fact observed by field measurements that cavities at the top points are very rare.

The absence of plastic deformation zones at the top point is because the normal compressive stresses dominate there. As a result, it is difficult to achieve the ratio between the normal and shear stresses, which can lead to plastic deformations. Some similar processes are observed at the bottom point of the tunnel, where, as seen from the model, no plastic deformation zones are observed.

Simultaneously, near the left and right sides of the tunnel, the ratio between the normal and shear stresses is such that plastic deformation zones can be observed. Cavities in the space behind the lining at these points occur most frequently as reflected in the results of the geophysical surveys.

The fact that the presence of cavities at points n = 2 and 4 is observed significantly less frequently than at points n = 1 and 5 can be explained by various additional factors. In particular, by analysing Fig. 3b, we can note that the highest peaks of ε_{pl} are offset downwards. In addition, vibrations from passing trains may have a large impact, especially in the lower side zones of the tunnel.

Thus, the joint interpretation of the modeling results and acoustic survey data in the tunnel shows their satisfactory convergence. The specifics of the stress–strain behavior can be deemed an important cause of cavities in the space behind the lining.

Conclusions

1. The common and frequent cases of cavity formation in the space behind the tunnel lining, such as deficient grouting, train-induced vibrations, etc. can be added with the stress–strain behavior of soil and plastic destruction at the soil–lining.

2. Multiple geophysical field studies using the impulse response method show cavity locations with their frequent occurrence in the lower tunnel zones. Cavities in the upper zones of the tunnel are significantly less common. Finally, there are almost no cavities at the top of the tunnel.

3. According to the results of the finite element modeling, it can be noted that the areas of plastic soil deformation also concentrate near the lower side tunnel zones and are less pronounced in the upper side zones.

4. The satisfactory convergence of the field measurement and modeling results suggests that the stress–strain behavior and plastic deformation of soil are the important factors in cavity formation in the space behind the tunnel lining. The stress–strain behavior also changes the acoustic properties of the soil/lining contact when switching from an undeformed state of the space behind the lining to the plastically deformed state, and affects the acoustic response to the impact action during testing.

Acknowledgments

This study was supported by the Russian Foundation for Basic Research, Grant No. 20-05-00341. The authors thank R. M. Gaisin and P. V. Nikolenko for the help in geophysical surveys in tunnels.

References

1. Jifei W., Hongwei H., Xiongyao X. et al. Void-induced liner deformation and stress redistribution. *Tunneling and Underground Space Technology*. 2014. Vol. 40. pp. 263–276.
2. Leung, C., Meguid, M. A. An experimental study of the effect of local contact loss on the earth pressure distribution on existing tunnel linings. *Tunneling and Underground Space Technology.* 2011. Vol. 26. pp. 139–145.
3. Kamel T., Limam A., Silvani C. et al. Modeling the degradation of old subway galleries using a continuum approach. *Tunneling and Underground Space Technology*. 2016. Vol. 48. pp. 77–93.
4. Vu M. N., Broere W., Bosch J. Volume loss in shallow tunneling. *Tunneling and Underground Space Technology*. 2016. Vol. 59. pp. 77–90.
5. Wu H., Shen S., Yang J. Identification of Tunnel Settlement Caused by Land Subsidence in Soft Deposit of Shanghai. *Journal of Performance of Constructed Facilities*. 2017. Vol. 31. DOI:10.1061/(ASCE)CF.1943-5509.0001082
6. Camos C., Spackova O., Straub D. et al. Probabilistic approach to assessing and monitoring settlements caused by tunneling. *Tunneling and Underground Space Technology.* 2016. Vol. 51. pp. 313–325.
7. Jinlong L., Hamza O., Davies-Vollum S. K. et al. Repairing a shield tunnel damaged by secondary grouting. *Tunneling and Underground Space Technology*. 2018. Vol. 80. pp. 313–321.
8. Li C., Li M. J., Zhao Y. G. et al. Layer recognition and thickness evaluation of tunnel lining based on ground penetrating radar measurements. *Journal of Applied Geophysics.* 2011. Vol. 73, Iss. 1. pp. 45–48.
9. Andrianov S. V. GPR monitoring of space between lining and rock in underground mines. *GIAB*. 2019. Iss. 5. pp. 124–132.
10. Kravitz B., Mooney M., Karlovsek J. et al. Void detection in two-component annulus grout behind a pre-cast segmental tunnel liner using Ground Penetrating Radar. *Tunneling and Underground Space Technology.* 2019. Vol. 83. pp. 381–392.
11. Chang C. W., Lin C. H., Lien H. S. Measurement radius of reinforcing steel bar in concrete using digital image GPR. *Construction and Building Materials.* 2009. Vol. 23. pp. 1057–1063.
12. Nabatov V. V., Gaisin R. M. Ground penetrating radar-assisted determination of reinforcement parameters for engineering structures and subway tunnels : Range of problems and handicaps. *GIAB*. 2014. No. 12. pp. 168–175.
13. Shilin A. A., Kirilenko A. M., Znajchenko P. A. Ground penetrating radar data interpretation for soil bodies in urban conditions. *Transport Construction*. 2015. No. 6. pp. 19–23.
14. Lu G., Zhao W., Fortec E. et al. Multi-frequency and multi-attribute GPR data fusion based on 2-D wavelet transform. *Measurement*. 2020. Vol. 166. DOI:10.1016/j.measurement.2020.108243
15. Schmalz B., Lennartz B. Analyses of soil water content variations and GPR attribute distributions. *Journal of Hydrology*. 2002. Vol. 267, Iss. 3(4). pp. 217–226. DOI:10.1016/S0022-1694(02)00152-X
16. Forte E., Pipan M., Casabianca D. et al. Imaging and characterization of a carbonate hydrocarbon reservoir analogue using GPR attributes. *Journal of Applied Geophysics*. 2012. Vol. 81. pp. 76–87.
17. Fedorova L. L., Sokolov K. O., Savvin D. V. et al. Analysis of Variance Amplitudes of Signals for Detecting Stuctural Permafrost Heterogeneities. *Proceedings of the 15th International Conference on Ground Penetrating Radar*. Brussels : GPR, 2014. pp. 301–305.
18. Denisov R. R., Kapustin V. V. Computerized georadar data processing. *Geofizika.* 2010. No. 4. pp. 76–80.
19. Sokolov K. O. Frequency-time presentation of georadar profiles based on continuous wavelet transform. *Journal of Mining Science*. 2014. Vol. 50, No. 2. pp. 256–259.
20. Azari H., Nazarian S., Yuan D. Assessing sensitivity of impact echo and ultrasonic surface waves methods for nondestructive evaluation of concrete structures. *Construction and Building Materials*. 2014. Vol. 71. pp. 384–391.
21. Wimsatt A., White J., Leung C. et al. Mapping Voids, Debonding, Delaminations, Moisture, and Other Defects Behind or Within Tunnel Linings. SHRP2 Renewal Research. Washington, DC : The National Academies, 2013.

22. Davis A. G., Lim M. K., Petersen C. G. Rapid and economical evaluation of concrete tunnel linings. *NDT and E International*. 2005. Vol. 38. pp. 181–186.
23. Baukov Yu. N., Baukov A. Yu. Vibro-acoustic control in mining and construction. Moscow : MGGU, 2006. 118 p.
24. Song K., Cho G. Bonding state evaluation of tunnel shotcrete applied on to hard rocks using the impact-echo method. *NDT and E International*. 2009. Vol. 42. pp. 487–500.
25. Chaudhary M. Effectiveness of Impact Echo testing in detecting flaws in prestressed concrete slabs. *Construction and Building Materials*. 2013. Vol. 47. pp. 753–759.
26. Meguid M. A., Dang H. K. The effect of erosion voids on existing tunnel linings. *Tunneling and Underground Space Technology.* 2009. Vol. 24. pp. 278–286.
27. Yasuda N., Tsukada K., Asakura T. Elastic solutions for circular tunnel with void behind lining. *Tunneling and Underground Space Technology*. 2017. Vol. 70. pp. 274–285.
28. Li Z., Zheng J., Wang R. Effects of grouting voids on the elastic buckling of confined pipe liners subjected to uniform pressure. *Thin-Walled Structures*. 2019. Vol. 137. pp. 502–514.
29. Wu H. N., Shen S. L., Chen R. P. et al. Three-dimensional numerical modelling on localized leakage in segmental lining of shield tunnels. *Computers and Geotechnics*. 2020. Vol. 122. DOI: 10.1016/j.compgeo.2020.103549
30. Ochmański M., Spacagna R. L., Modoni G. 3D numerical simulation of consolidation induced in soft ground by EPB technology and lining defects. *Computers and Geotechnics.* 2020. Vol. 128. DOI: 10.1016/j.compgeo.2020.103830
31. Yasuda N., Tsukada K., Asakura T. Three-dimensional seismic response of a cylindrical tunnel with voids behind the lining. *Tunneling and Underground Space Technology*. 2019. Vol. 84. pp. 399–412.
32. Yau K., Paraskevopoulou C., Konstantis S. Spatial variability of karst and effect on tunnel lining and water inflow. A probabilistic approach. *Tunneling and Underground Space Technology*. 2020. Vol. 97. DOI: 10.1016/j.tust.2019.103248
33. Huang Q., Huang H., Ye B. et al. Evaluation of train-induced settlement for metro tunnel in saturated clay based on an elasto-plastic constitutive model. *Underground Space (China).* 2018. Vol. 3. pp. 109–124.
34. Ruiz J. F., Soares P. J., Alves C. P. et al. The effect of tunnel construction on future underground railway vibrations. *Soil Dynamics and Earthquake Engineering*. 2019. Vol. 125. DOI: 10.1016/j.soildyn.2019.105756
35. Voznesenskii A. S., Nabatov V. V. Identification of filler type in cavities behind tunnel linings during a subway tunnel surveys using the impulse-response method. *Tunneling and Underground Space Technology*. 2017. Vol. 70. pp. 254–261.
36. Nabatov V. V. Detection of voids behind lining in metro tunnels by spectral attributes of Q-factor in the lining–soil system vibrations. *Gornyi Zhurnal.* 2019. No. 7. pp. 67–70. DOI:10.17580/gzh.2019.07.03
38. Nazarova L. A. Estimating the stress and strain fields of the Earth's crust on the basis of seismotectonic data. *Journal of Mining Science*. 1999. Vol. 35, No. 1. pp. 26–35. EM